70-m Ka-Band Implementation Study

Daniel Hoppe*

ABSTRACT. — This article describes results from simulation work related to future operation of the 70-m antennas in the 30-GHz band. It identifies the primary gain loss mechanisms related to the quality of the radio frequency (RF) surface and pointing errors as well as various methods for rectifying these losses. It uses detailed RF models to estimate the antenna performance both with and without compensation applied, and depicts example layouts of the additional surfaces and mechanisms required in the RF path. Finally, it outlines future work.

I. Introduction

This article describes results from simulation work related to the addition of a Ka-Band capability in the 70-m antennas, considering both the DSN Ka-bands: transmit (34.2–34.7 GHz) and receive (31.8–32.3 GHz). Such an upgrade will be challenging and must address the primary gain loss mechanisms related to the quality of the radio frequency (RF) surface and pointing errors. These loss mechanisms and the methods for dealing with them are described in separate sections. In each case, detailed RF antenna models were created to simulate the nominal gain loss and residual loss after corrective measures are taken. The article concludes with some suggestions for future work.

II. Motivation and History

Recent DSN loading studies indicate that additional aperture area will be needed to meet future mission needs.[1] Adding the Ka-band capability to the 70-m antennas is likely to be one of the most cost-effective ways to provide the additional aperture area. The operation of the largest DSN antennas at Ka-band was first described by Potter in 1980 [1]. In 1999, a demonstration of Ka-band operation at DSS-14 was completed.[2,3] It was focused on demonstrating two gravity compensation techniques— a deformable mirror (DM) and an

[1] "DSN Futures Study Report," Stephen M. Lichten, Internal JPL Document, August 7, 2024.

[2] "'70m Ka-Band Implementation Study," D. J. Hoppe, JPL D-19434, January 10, 2000.

[3] "Ka-Band DFP/AFCS Demo on the 70-M," D. J. Rochblatt, July 29, 1999.

* Ground Communications & Architectures.

The research described in this publication was carried out by the Jet Propulsion Laboratory, California Institute of Technology, under a contract with the National Aeronautics and Space Administration (80NM0018D0004). © 2026 California Institute of Technology. U.S. Government sponsorship acknowledged.

array feed. No further work in this area, including modeling, was done after the 1999 demonstration.

III. Basic Considerations for Ka-Band Operation of the DSN 70-m Antennas

Figure 1 shows the main contributors to gain loss (aperture efficiency) of any large DSN antenna. Contributors that are not the primary concern of this report, since they are not a discriminating loss for Ka-band relative to S- and X-band on the 70-m antennas, are in black boxes in the figure. The first of these losses is physical optics loss, which depends on the quality of the dual reflector shaping and its ability to transform the tapered feed pattern into a uniform amplitude and uniform phase distribution at the exit aperture of the primary reflector. Physical optics is generally a computed quantity and is typically 92%, and it is largely independent of frequency, assuming appropriate feeds are used in each band. Ohmic loss is due to the finite conductivity of all the surfaces the RF energy encounters. This loss increases with frequency and amounts to a loss of approximately 0.1% per reflection at Ka-band. Strut blockage represents a loss of approximately 8% and is independent of frequency. Finally, primary and secondary Ruze loss is due to the finite manufacturing accuracy of all the surfaces in the antenna, primary panels, secondary panels, and any reimaging optics. For a fixed surface quality, this loss increases with frequency. Fortunately, the 70-m secondary and primary panels are manufactured to the same quality as the beam waveguide (BWG) antennas, making this loss factor important but not a driving loss mechanism at Ka-band on the 70-m antenna. This is described in more detail in Section V on antenna surface errors.

Major contributors to 70-m loss at Ka-band are in red boxes in the figure. The first of these loss mechanisms is Ruze loss due to the quality of the primary panel set at the rigging angle. With the current panel set, this is a major loss contributor at Ka-band for the 70-m antennas. The panel setting must be improved using holography prior to implementation of any of the other items addressed in this report, such as gravity compensation and pointing. It is possible that improvements to the existing holography methods may be necessary to achieve this. The distortion of the antenna as it tips in elevation, gravity deformation Ruze loss, is also a significant loss mechanism at Ka-band. This article studies in detail the addition of reimaging optics and deformable surface in the Ka-band path to correct for gravity effects. Due to the narrow beamwidth at Ka-band on the 70-m antenna, pointing is a challenge, as indicated in the figure. While initial system alignment is accomplished using metrology and holography, the use of a scan mirror and monopulse feed at Ka-band is studied as a correction method for simple but dynamic pointing errors. This scan mirror is placed in a location where both the transmit and receive beams will be scanned together. Finally, because of the narrow beamwidth, it will often be necessary to offset the transmit and receive beams (point-ahead). This is handled on the 34-m antennas by placing the transmitter on a moving platform. This article studies solving this problem with the use of an independent scan mirror in the Ka-band transmit path only, allowing for the transmit and receive beams to be offset in space.

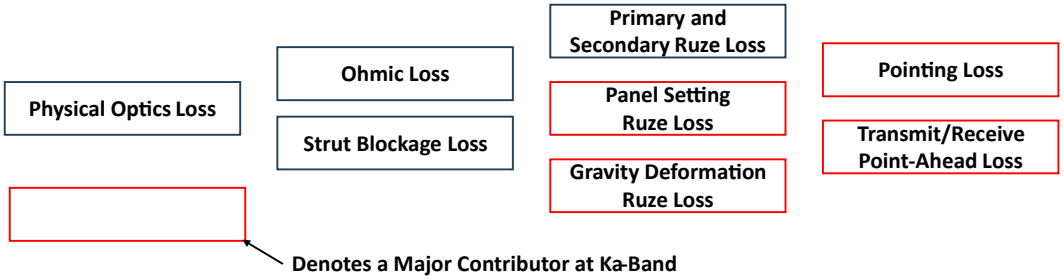


Figure 1. Contributors to 70-m Ka-band gain performance.

IV. GRASP Antenna Model

As part of this work, a complete model of the 70-m antenna was developed in GRASP [2]. The basic 70-m antenna geometry is depicted in Figure 2. A simple Gaussian feed model was used in all GRASP models. Both the primary and secondary surfaces are shaped to produce a uniform amplitude and uniform phase distribution in the exit aperture of the primary. A rotationally symmetric primary, which is a slightly perturbed parabola, is used (Figure 3). The surface is described numerically using a large table in the DSN drawing set. Since the 70-m feeds are local on a focal ring, the secondary is an asymmetric surface (Figure 4). As shown in the figure, the surface is described using eight cuts, which are included in the DSN drawing set for the antenna (left panel). These cuts are then interpolated in radius and subsequently interpolated in angle using a Fourier series to create the numerical 3-D surface used in GRASP (right panel). All indications are that the numerical description of the primary surface adequately models the antenna at Ka-band. However, numerical tests of the secondary surface indicate that some slight gain loss is present due to numerical inaccuracy in the representation of this surface. This is likely due to the interpolation methods used to create the GRASP surface file. The slight gain loss is of little consequence in the study results, shown in the remainder of the report, which involve relative gain losses on the antenna due to gravity and beam scanning.

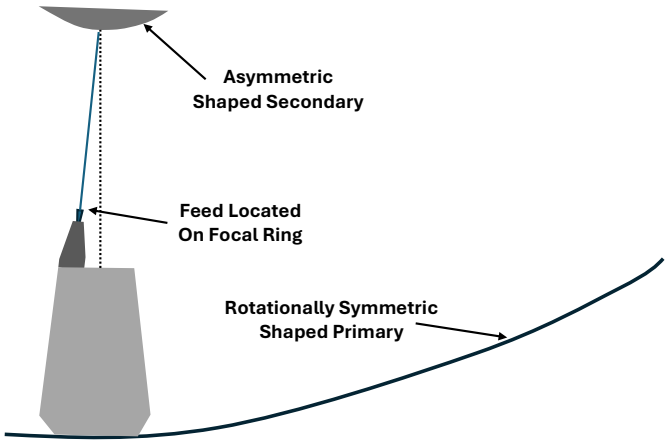


Figure 2. DSN 70-m antenna geometry.

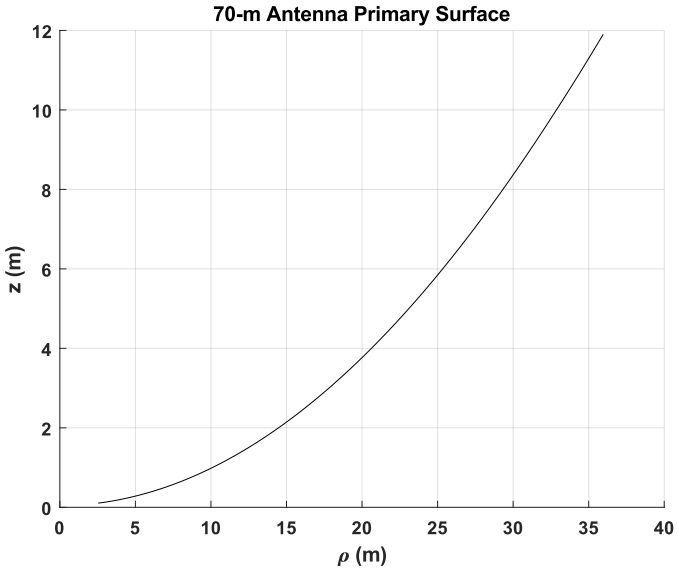


Figure 3. Circularly symmetric primary surface.

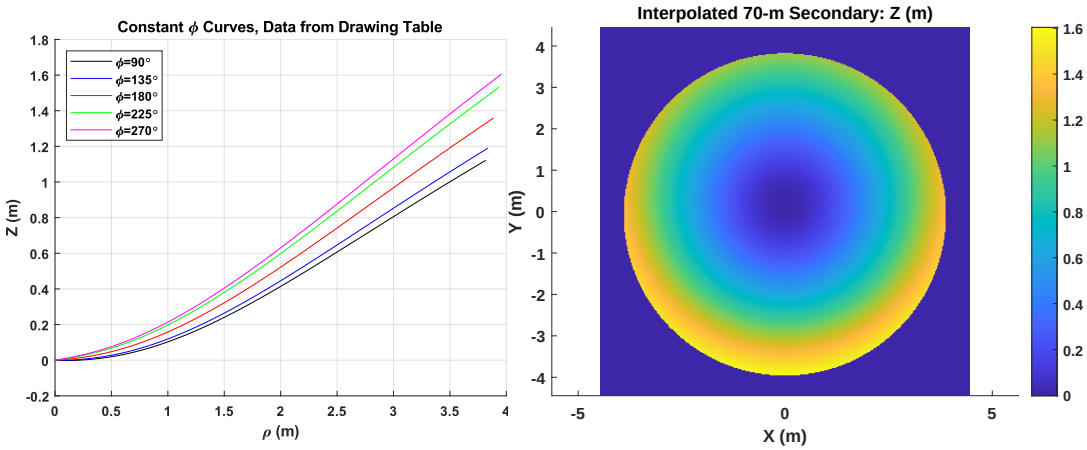


Figure 4. Asymmetric secondary surface.

Figure 5 shows the complete GRASP model, and Figure 6 shows the computed radiation patterns at 8.45 GHz (top panel) and 32 GHz (bottom panel).

Patterns in both bands have excellent symmetry and are consistent with nearly uniform illumination at the primary exit plane. The computed gain values are 75.39 dBi at X-band and 86.79 dBi at Ka-band, corresponding to physical optics aperture efficiencies of 90.0% and 86.7%.

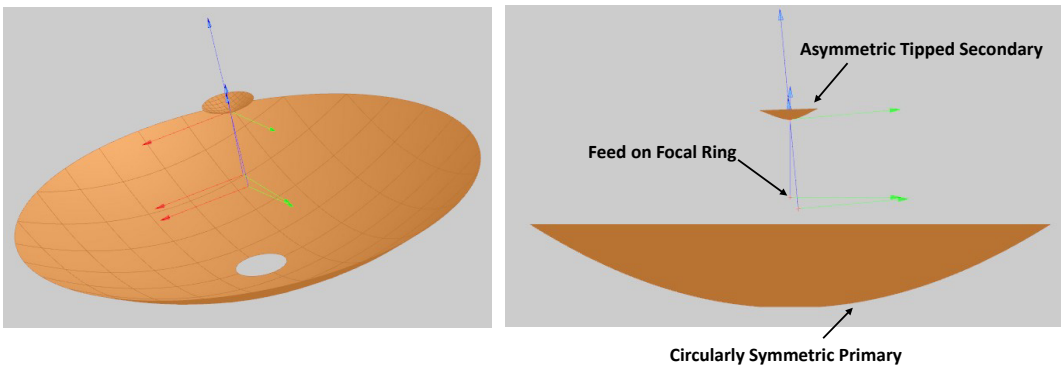
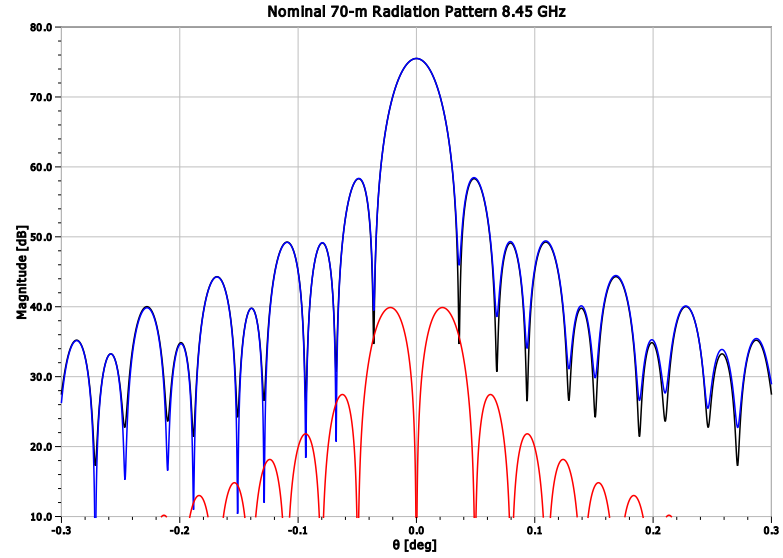


Figure 5. GRASP antenna model.



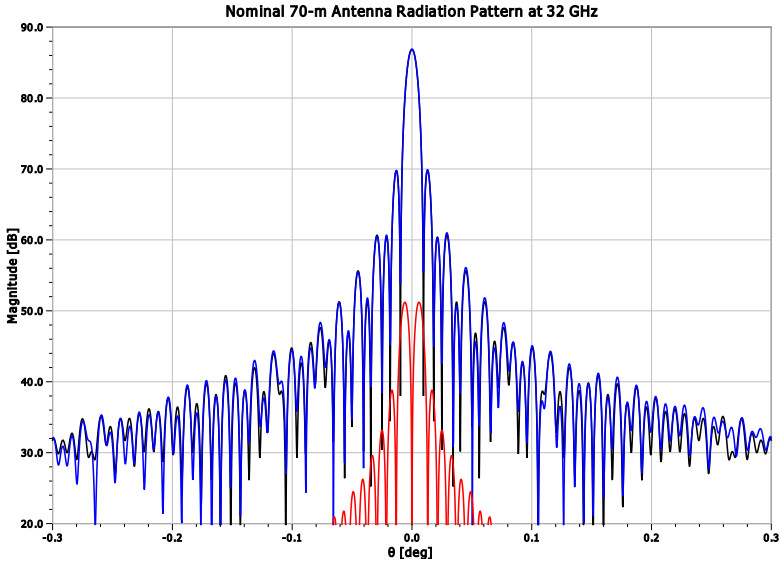


Figure 6. Computed radiation patterns, nominal antenna geometry.

V. Antenna Surface Errors

This section considers the gain loss contributions due to surface manufacturing and the finite accuracy to which the primary surface panels can be set. Table 1 and Table 2 tabulate the losses at the uppermost frequency in the receive and transmit Ka-bands. The contributors to these losses correspond to the complete optics needed for a transmit/receive system with gravity compensation, vernier pointing of both transmit and receive beams as a group to correct for overall pointing error, and differential pointing of the transmit beam relative to the receive beam (point ahead). These layouts are described in detail in Section X of this article.

The tables assume the surface error is 0.127 mm (0.005 in.) for the primary panels and 0.1524 mm (0.006 in.) for the secondary surface, as specified in the DSN drawing package. All additional surfaces are assumed to have the same root mean square (RMS) as the primary panels, a value that is also consistent with the current 34-m BWG antenna reimaging optics. The overall set of the 70-m panels is an open question, and its contribution is considered separately in Figure 7.

At the top of the receive band, the secondary contributes approximately 0.185 dB of loss, and each of the remaining surfaces contributes 0.128 dB. The overall loss excluding the panel set is 0.827 dB, for an efficiency of 82.7%. In the higher-frequency transmit band, the secondary loss is 0.213 dB, and the other surfaces are 0.148 dB for an overall loss of 0.954 dB and an efficiency of 80.3%.

Table 1. Surface RMS losses in a typical Ka-band receive path, 32 GHz.

RMS Contributor	RMS Path Error (mm)	Ruze Efficiency	Ruze Loss (dB)	Source
70-m Primary	0.1270	0.9709	0.1284	DWG 9486761
70-m Secondary	0.1524	0.9583	0.1849	DWG 9486728
Reimaging Ellipse	0.1270	0.9709	0.1284	Assumption
Deformable Mirror	0.1270	0.9709	0.1284	Assumption
Transmit/Receive FSS	0.1270	0.9709	0.1284	Assumption
Receive Ellipse	0.1270	0.9709	0.1284	Assumption
70-m Set	0.0000	1.0000	0.0000	See Figure 7
Total		0.8266	0.8269	

Table 2. Surface RMS losses in a typical Ka-band transmit path, 34.7 GHz.

RMS Contributor	RMS Path Error (mm)	Ruze Efficiency	Ruze Loss (dB)	Source
70-m Primary	0.1270	0.9665	0.1482	DWG 9486761
70-m Secondary	0.1524	0.9521	0.2134	DWG 9486728
Reimaging Ellipse	0.1270	0.9665	0.1482	Assumption
Deformable Mirror	0.1270	0.9665	0.1482	Assumption
Transmit Ellipse	0.1270	0.9665	0.1482	Assumption
Transmit Flat	0.1270	0.9665	0.1482	Assumption
70-m Set	0.0000	1.0000	0.0000	See Figure 7
Total		0.8027	0.9544	

Efficiency losses due to the finite ability to set the panels on the 70-m antenna is a significant factor and carries some risk. As shown in Figure 7 (left panel) the current estimated panel set on DSS-63 is approximately 1.2 mm,[4] which translates to an enormous Ruze loss of more than 10 dB at Ka-band. Other points of note in the figure are the initial set at DSS-13,[5] the first serious attempt to obtain Ka-band quality (approximately 0.9 mm), the final achieved set at DSS-13 (0.45 mm), and the high-quality panel set at DSS-24 (0.25 mm).[6] A zoomed version of the data is shown in the right panel, where only the two best set points are included.

It is unclear whether a 0.25-mm panel set is possible on the 70-m antennas. In addition, whether there is a gradual degradation of the panel set on the 70-m antennas vs. time is an outstanding question. More study is needed in these areas: ultimate panel set achievable on the 70-m and expected stability of the surface vs. time. For these reasons and based on current limitations, it seems a best-case panel set of 0.25 mm is possible, resulting in 0.5 dB of gain loss. A worst-case value of 0.35 mm, somewhat better than the DSS-13 final value, might be reasonable, resulting in 1 dB of loss due to the panel set.

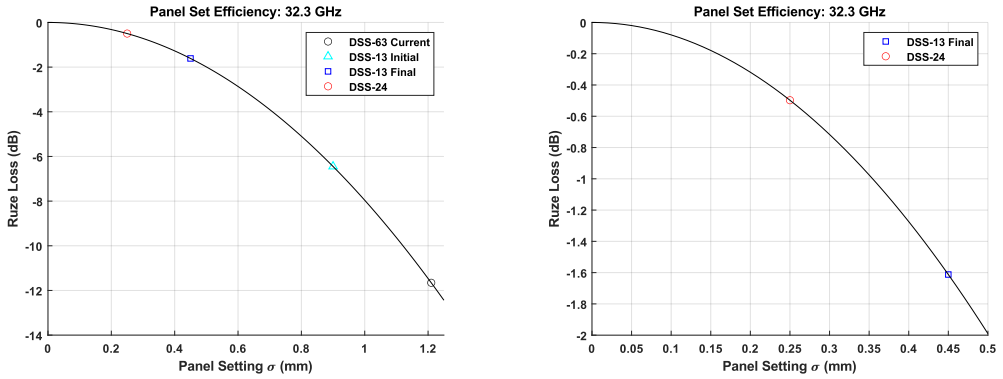


Figure 7. Ruze loss due to panel set.

VI. Gravity Effects

The most significant contributor to 70-m antenna gain loss at Ka-band is the gravity deformation of the antenna as it tracks through elevation. Without compensation, this loss can be as high as a few decibels when the elevation is near zenith or the horizon, far from the rigging angle near 45°.

The exact gravity distortion on any large antenna is difficult to measure accurately. Some variation in the surface distortion across the three DSN 70-m antennas is to be expected as well. This article uses a data set from 2023 of connected interferometry holography measurements of DSS-63, as described in [3]. Using this representative data set and the GRASP model described earlier, this article assesses the performance of various compensation methods as described in Sections VII and VIII.

---

[4] "DSS 63 Holography," J. Cucchissi, L. Locke, D. Rochblatt, H. Soldan, A. Torre, and M. Vazquez, September 18–29, 2023.

[5] "DSS-13 Beam Waveguide Antenna Project: Phase 1 Final Report," M. Britcliffe, JPL D-8451, May 15, 1991.

[6] "DSS-24 Antenna RF Performance Measurements," M.J. Britcliffe, JPL-D 890-270, February 1, 1995.

Figure 8 shows the DSS-63 holography surface maps obtained for various elevation angles. The maps shown are difference maps, where the 43.5° data was used as the rigging angle and all raw data sets had the 43.5° data set subtracted. The maps are shown with a common range of +/- 2 mm, and, as expected, the difference map at 43.5° is identically zero. The maps clearly display the well-known astigmatic form of distortion, which is odd with respect to the rigging angle. The distortion files have also been masked in the shadow area of the struts where the holography signal-to-noise ratio is too weak to sense the distortion. Finally, there is an artifact in the 62.5° data set that produces a copy of the strut shadow. None of the effects relating to the strut shadow region were found to be significant, and results obtained with the masks in place or using the raw data under the mask were similar overall.

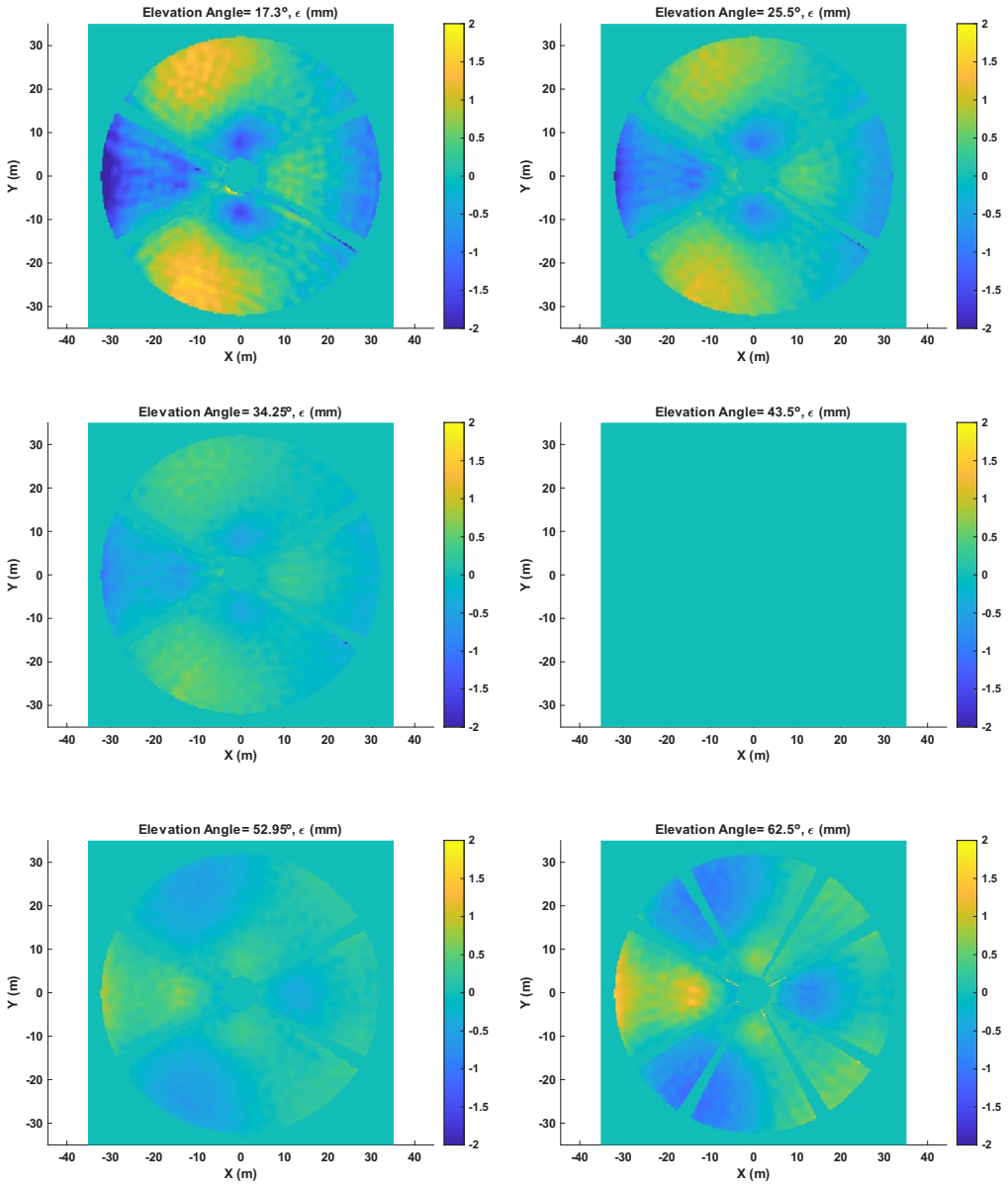


Figure 8. DSS-63 holography measurements.

VII. Gravity Compensation: Deformable Secondary

This section describes the results for one possible implementation of gravity compensation using a deformable surface. This case considers the possibility of distorting the RF secondary in a manner that corrects for the distortion on the primary as the antenna tracks in elevation. Such a system has been implemented on many optical and RF telescopes, with one example being the MIT Haystack antenna [4].

Distorting the secondary for compensation has several advantages relative to introducing a compensating mirror using reimaging optics. In the high frequency limit compensation using the secondary can correct the distortion at all frequencies at once in different bands and for both transmit and receive. Since the secondary is large, the distortions are gradual, requiring small slopes in the surface. Using the secondary also eliminates the need for additional optics, minimizing the required changes to the RF paths in the antenna and saving space. Disadvantages include modifying an already complex, shaped surface and operating the deformable surface in an uncontrolled environment. In addition, the ideal placement of the deformable surface is at an optical pupil plane, and the secondary is not at this ideal location. The next section studies a deformable flat plate, which offers the complementary set of advantages and disadvantages.

Figure 9 is a rough pictorial representation of the deformable secondary modeling in GRASP. The major steps in the modeling are, in sequence:

(1) Apply the gravity distortion to the primary surface in GRASP.

(2) Use the ray tracing capability in GRASP to obtain the ray trajectories from the feed focus through both the secondary and primary. Ideally, all rays should have the same total ray path length (left panel).

(3) Find the mean phase front exiting the primary and compute the path length error relative to the mean for each ray. This step is carried out in Matlab (left panel).

(4) Use the path length error for each ray along with the incident angle on the secondary surface to compute the surface distortion, $\varepsilon(x,y)$, necessary on the secondary to correct the phase front. This step is carried out in Matlab.

(5) Create a distortion file for the secondary in GRASP format.

(6) Finally, run GRASP in Physical Optics mode with both the primary distortion and secondary distortion (compensation) in place to determine the effectiveness of the compensation (right panel).

In this approach, the required secondary compensation is computed using ray tracing only, and its effectiveness is therefore optimum in the high-frequency regime, where diffraction effects are minimal. The final calculated performance is obtained using GRASP and Physical Optics, and includes all diffraction effects.

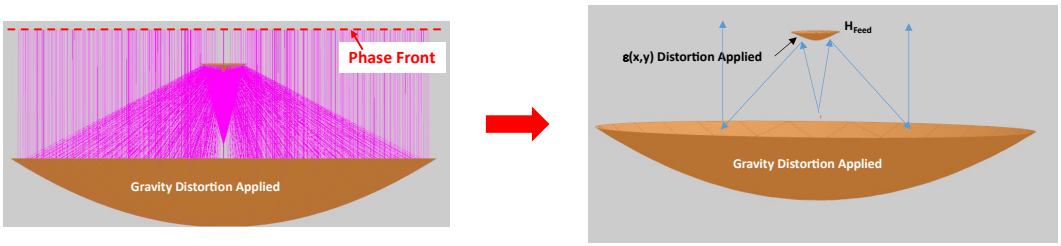


Figure 9. Deformable secondary and surface construction.

Figure 10 shows the primary surface distortion at 17.3° elevation (left panel) and the compensating distortion necessary on the secondary computed using ray tracing as described above (right panel). The astigmatic profile of both the primary distortion and the compensating distortion on the secondary are clearly visible. In this study, unmasked gravity distortions were used, which leads to somewhat more gain loss, particularly at the extreme elevation angles, relative to using the masked distortions.

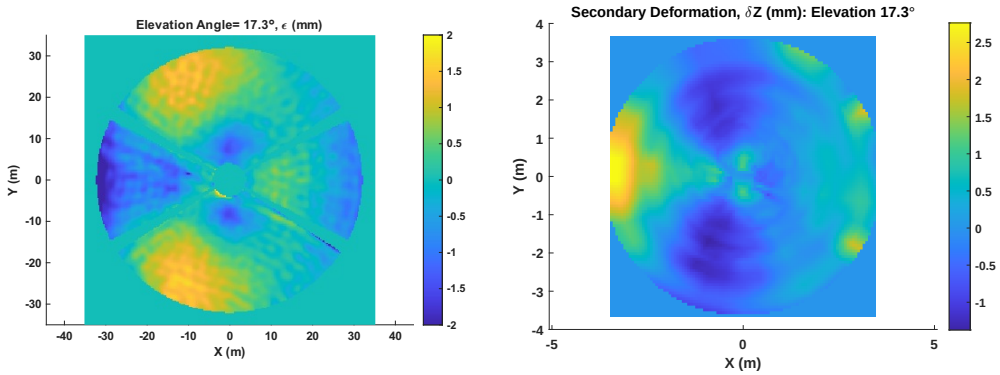


Figure 10. Deformable secondary surface, 17.3°.

The six-step process described above is repeated for the available elevation distortions and the antenna gain both with and without the secondary distortion in place to access the compensation's performance. Calculations are made at both X-band and Ka-band. Note that the 43.5° rigging angle data serves as a control point where both distortion and compensation are zero.

Figure 11 shows the effectiveness of the deformable secondary at X-band. The uncompensated gain loss is modest at this frequency, with a maximum loss of around 0.2 dB at the lowest elevation angles. Compensation can recover most of this gain loss at low elevation angles and approximately one-half of the loss at high angles. At this frequency, it is likely that compensation is limited by diffraction effects, which are not included in the ray tracing used to determine the required secondary surface distortions. Given the low uncompensated loss at X-band and the achievable compensation, minimal impact on overall antenna performance at X-band is expected.

Figure 12 shows the effectiveness of the deformable secondary at Ka-band. At Ka-band the uncompensated gain loss is quite significant, reaching a maximum loss of around 2.7 dB at the lowest elevation angles. Compensation can recover most of this gain loss at low elevation angles, reducing the loss from 2.7 to 0.2 dB, and can reduce the loss to 0.4 dB at

high elevation angles. At this frequency, diffraction effects on the compensation are less significant, and excellent performance is obtained.

It should be noted that this model uses an idealized compensating surface, and in practice, the deformation will be created with a finite number of actuators, limiting the ability to match the ideal surface. This can be studied with the same methods once the mechanical design is complete and its limitations are known.

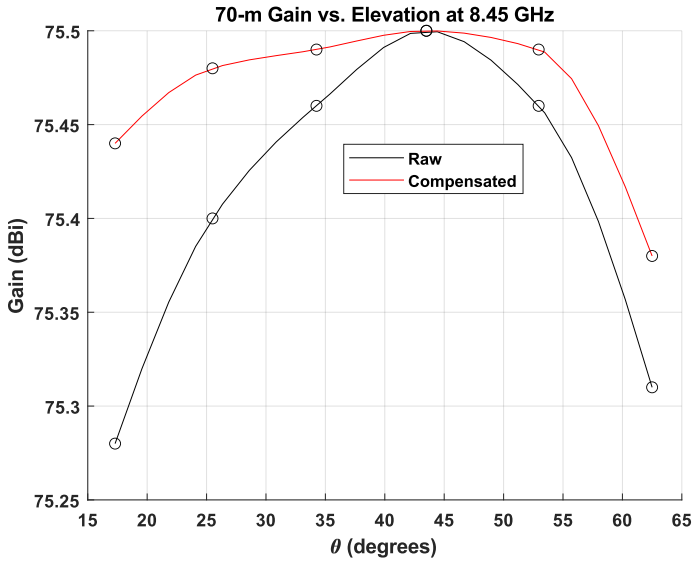


Figure 11. Deformable secondary compensation, X-band.

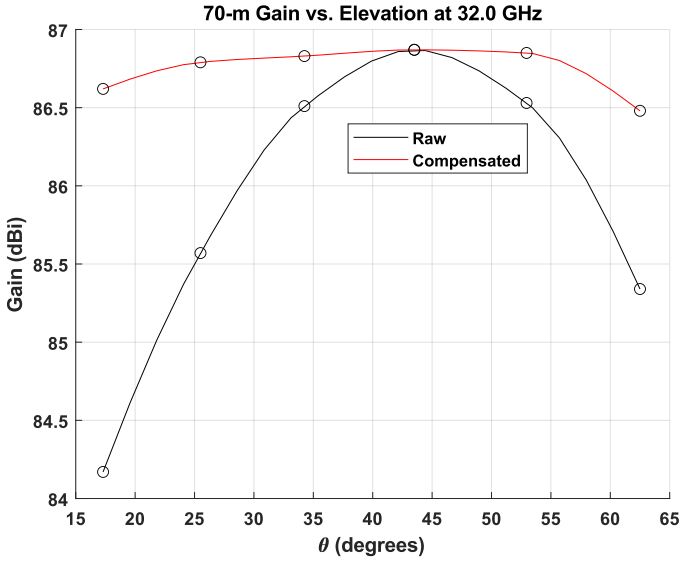


Figure 12. Deformable secondary compensation, Ka-band.

VIII. Gravity Compensation: Flat Deformable Mirror (DM)

This section considers the possibility of using reimaging optics and a flat DM to correct for the distortion on the primary as the antenna tracks in elevation. This is essentially the system that was demonstrated on DSS-14 in 1999 and later studied further through modeling [5,6].

Figure 13 is a pictorial representation of the flat DM modeling in GRASP. In this system, the original antenna focus is reimaged using an ellipse to a second focus where the feed is placed. A flat DM is located between the ellipse and the feed. The distance between the ellipse and the flat DM is chosen so that an optical pupil plane appears at the flat mirror. At this location, in the optical limit, the primary is exactly reimaged on the flat mirror. This implies that the distortions on the primary reappear exactly at the DM and a distortion of opposite sign should be 100% effective as compensation. At any plane other than this plane, the distortions on the primary are mixed into both phase and amplitude effects, and cannot be compensated by a phase shift only (flat surface distortion).

The disadvantages of this system include the need for additional optics, increased diffraction effects because of the smaller surfaces involved, and potential layout difficulties in the tri-cone area. The advantages include operation of a smaller deformable surface and doing so in a controlled environment. Finally, the ideal placement of the deformable surface at an optical pupil plane should produce excellent performance.

The major steps in the modeling are essentially the same as for the deformable secondary compensation but tracing through the reimaging optics and applying the compensation at the flat mirror. In sequence, the steps are:

(1) Apply the gravity distortion to the primary surface in GRASP.

(2) Use the ray tracing capability in GRASP to obtain the ray trajectories from the feed focus through the flat mirror, ellipse, secondary, and primary. Ideally, all rays should have the same total ray path length.

(3) Find the mean phase front exiting the primary and compute the path length error relative to the mean for each ray. This step is carried out in Matlab.

(4) Use the path length error for each ray, along with the incident angle on the flat mirror surface, to compute the surface distortion, $\varepsilon(x,y)$, necessary on the secondary to correct the phase front. This step is carried out in Matlab.

(5) Create a distortion file for the flat mirror in GRASP format.

(6) Finally, run GRASP in Physical Optics mode with both the primary distortion and flat mirror distortion (compensation) in place to determine the effectiveness of the compensation.

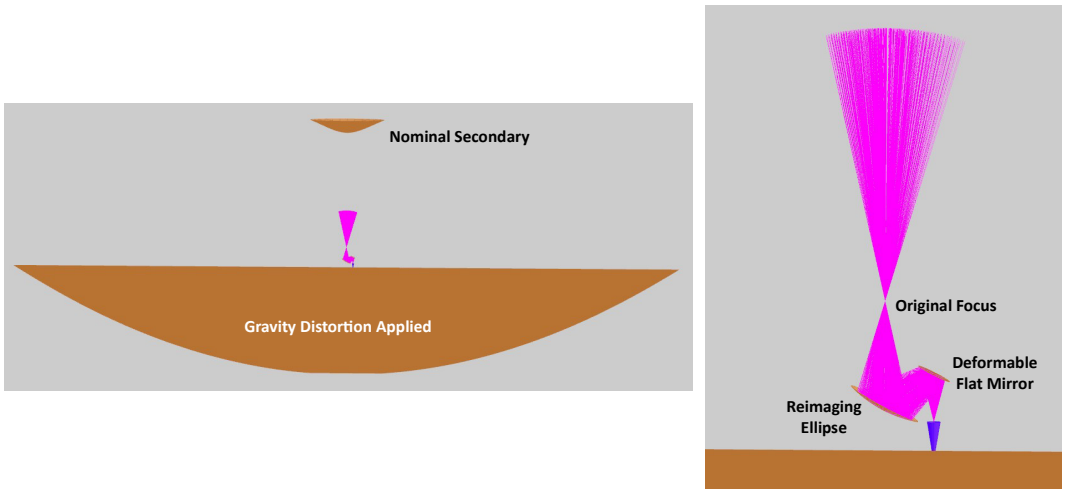


Figure 13. Flat DM compensation.

Figure 14 shows the primary surface distortion at 17.3° elevation (left panel) and the compensating distortion necessary on the flat mirror, once again computed using ray tracing as described above (right panel). As with the secondary compensation approach, the astigmatic profile of both the primary distortion and the compensating distortion on the secondary are clearly visible. In this study, the gravity distortion masks were used, which leads to somewhat less gain loss, particularly at the extreme elevation angles, relative to using the unmasked distortions.

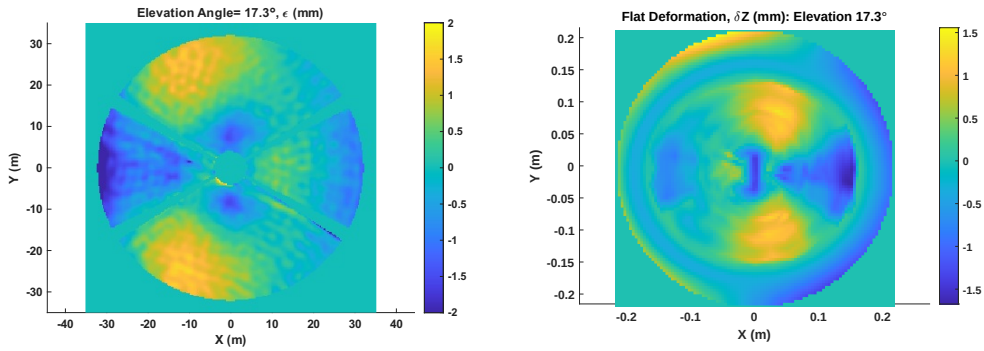


Figure 14. Deformable flat surface, 17.3°.

Figure 15 shows the effectiveness of the deformable flat at X-band. The uncompensated gain loss is modest at this frequency, with a maximum loss of around 0.2 dB at the lowest elevation angles. At this frequency, reimaging introduces diffraction effects, focus shift, etc., which are not included in the ray tracing used to determine the required flat surface distortions. As shown in the figure, the compensation is largely ineffective at X-band but does not cause significant degradation. As with the secondary compensation, given the low uncompensated loss at X-band, minimal impact on overall antenna performance at X-band is expected. Given additional study time, the diffraction effects at X-band could be observed further.

Figure 16 shows the effectiveness of the deformable flat at Ka-band. Compensation can recover most of the 2.1-dB gain loss at low elevation angles, reducing the loss from 2.7 to 0.35 dB, and can reduce the loss to 0.25 dB at high elevation angles. At this frequency, diffraction effects on the compensation are less significant, despite the small reimaging optics and flat, and excellent performance is obtained.

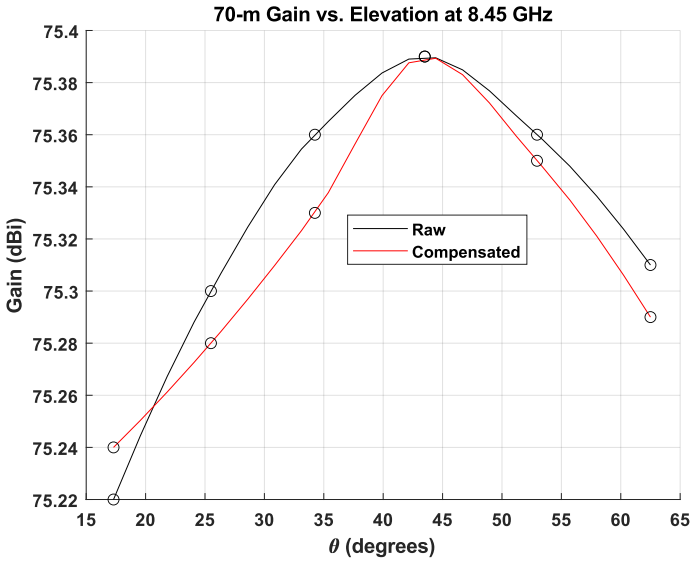


Figure 15. Deformable flat compensation, X-band.

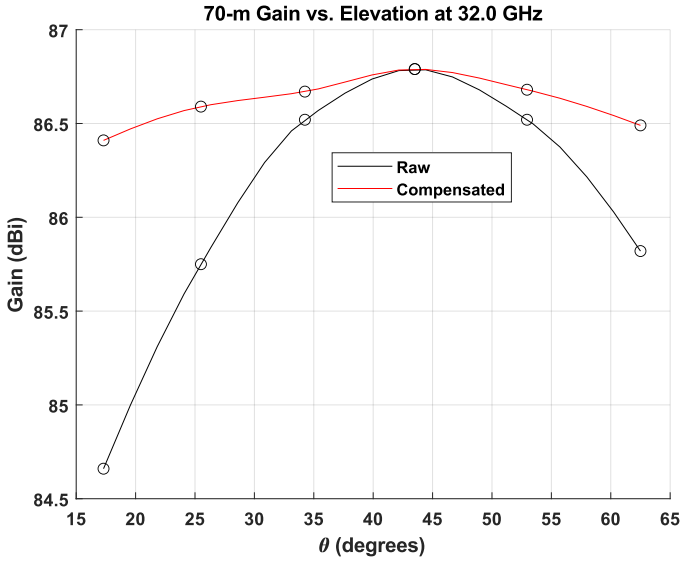


Figure 16. Deformable flat compensation, Ka-band.

The correct placement of the DM in the optical path is of utmost importance in order to optimize performance. The previous analysis used a position for the flat that was based on an idealized, approximate optical model of the 70-m dual reflector antenna. This chosen position was identical to that used in the experiments conducted at DSS-14 in 1999. Given the approximations involved in choosing this position, some study is warranted.

To study the optimum placement of the flat mirror, GRASP models were created for a variety of DM positions around the nominal position of 34.5 in. from the ellipse (Figure 17, left panel). For each model, a ray-based compensator was constructed and applied to recover the lost gain at 17.3° elevation and 32 GHz. The quality of the compensation is clearly a function of DM placement (right panel), with a position of 32.5 in. optimizing the compensation. There, all but 0.3 dB of the gain lost at 17.3° can be recovered.

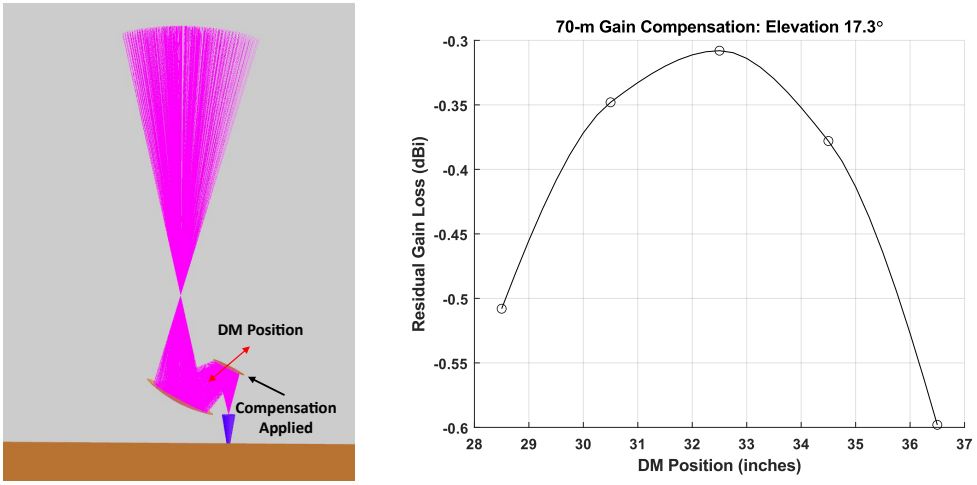


Figure 17. Deformable flat compensation vs. position, Ka-band, 17.3° elevation.

IX. Vernier Beam Steering

If implemented, operation of the 70-m antenna would lead to the most accurate pointing requirements in the DSN. Vernier pointing of the Ka-band beam without the need to move the entire 70-m structure would be of great benefit. Searching for a source, compensating for offsets between the X-band and Ka-band optics, and compensating for thermal effects and atmospheric effects would all benefit from a vernier pointing capability. This section discusses two methods for achieving vernier pointing: physically moving the feed in the focal plane using a scan platform and rotation of the flat DM (Figure 18).

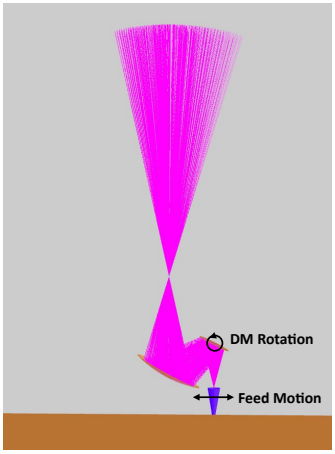


Figure 18. Beam steering methods.

Use of the rotating mirror has many advantages over a scan platform, such as the following: Rotation is typically preferred over linear motion in most applications; it can be achieved using an already existing optic without the need for more hardware; and in the case of a transmit beam, the amplifier may be difficult to physically move due to cabling, volume, and weight.

Both the rotating mirror and scanned feed systems were modeled in GRASP at 32 GHz, and typical scanned beams are shown in Figure 19 (mirror rotation, left panel; feed scan, right panel). As is evident from the figure, gain loss is associated with scanning the beam using either system. Figure 20 shows the antenna gain vs. beam position in degrees (left panel) and relative gain vs. beam position in Ka-band beamwidths (full width half maximum [FWHM]; right panel). The simulations show that for any amount of scan the rotating mirror outperforms the scanned feed. The current mean radial pointing error (MRE) of the 70-m antennas is approximately 2–3 mdeg [7], or less than ½ the Ka-band (FWHM). The plots below indicate the rotating mirror can scan the beam 1.5 full beamwidths at Ka-band and suffer only 0.5 dB of gain loss, and 2 beamwidths would suffer around 1 dB of loss.

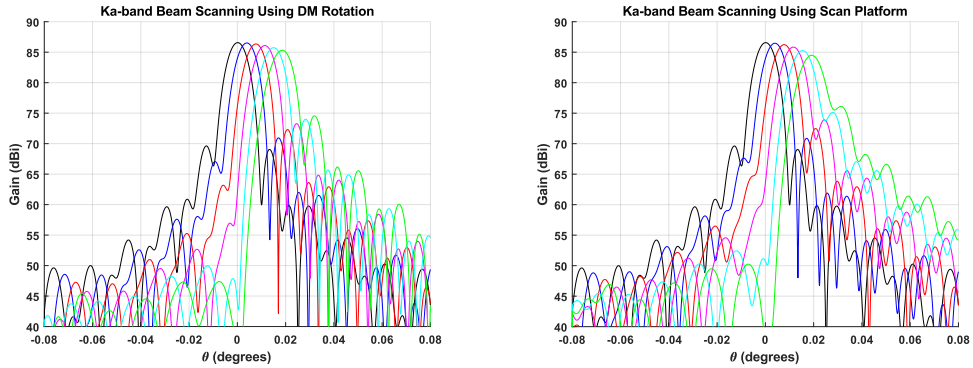


Figure 19. Scanned beams, Ka-band.

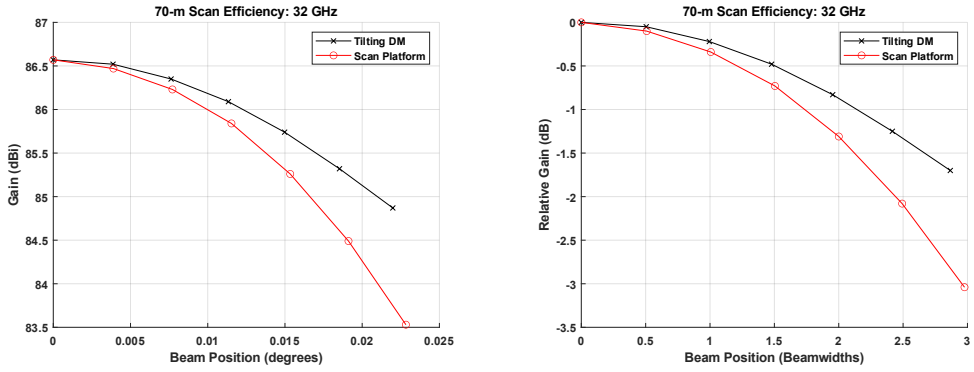


Figure 20. Scan loss, Ka-band.

X. Strawman Ka-Band Transmit/Receive Optical Layout

Although no mechanical layout work was completed in this study, a strawman optical design is depicted in Figure 21. The common optics include the main reimaging ellipse, the deformable flat, and a transmit/receive frame synchronizer subassembly (FSS). After reflecting off the FSS, the receive signal is reimaged into a receive monopulse feed (left panel). The transmit signal passes through the FSS, is reimaged by an ellipse, and reflects off a flat mirror into the transmit feed.

The flat DM is placed at a pupil plane as described earlier. In addition to correcting for gravity deformations in both the transmit and receive bands, it also is rotated to provide common mode vernier beam steering for both transmit and receive beams. The flat plate in the transmit path is also placed at a secondary pupil plane. This mirror may be rotated to offset the transmit beam with respect to the receive beam (point-ahead).

Although all the mirrors are shown in-plane in this layout, the FSS, receive ellipse, and transmit ellipse can all be rotated out of plane, providing many different layout options. For reference, in the 1999 experiment, the reimaging ellipse and deformable flat (the largest mirrors in the layout) were housed in a standard DSN cone. Although detailed layout work is needed, a solution that fits the strawman layout here inside a cone is likely attainable.

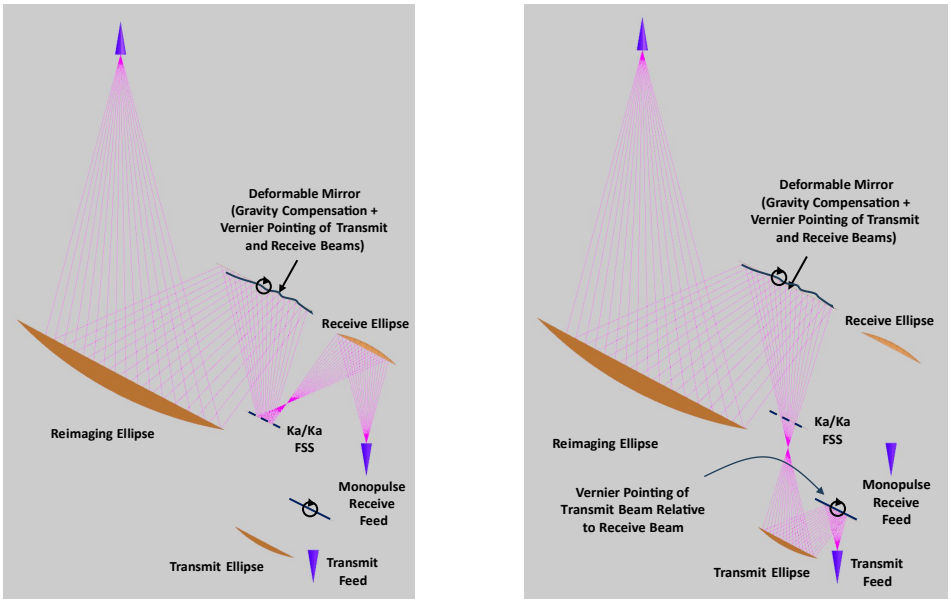


Figure 21. Transmit/Receive layout, Ka-Band.

XI. Overall Performance Summary

This section summarizes model results for the gain loss contributors shown in Figure 1.

Table 3 tabulates worst-case and best-case loss contributions for a deformable flat implementation of gravity compensation and use of a rotating mirror for point-ahead. For each contributor, a best-case and a worst-case value is shown in separate columns. The

best-case scenario assumes on-axis pointing at the rigging angle and an aggressive assumption for the quality of the primary panel set. The worst case assumes offset pointing of 2 beamwidths at a low elevation angle and a modest panel set. Here the offset pointing could be needed for point-ahead or other general antenna pointing errors.

Fixed values for physical optics loss and blockage loss apply to both the best- and worst-case scenarios. Fixed Ruze loss due to mirror surface quality is also identical for both scenarios. For panel set, the model assumes an aggressive value of 0.25 mm in the best case and 0.35 mm in the worst case. For gravity compensation, the model assumes perfect performance at the rigging angle and a residual loss value from the simulation at 17.3° elevation. Finally, the model assumes perfect pointing in the best case and in the worst case a pointing scan of two full beamwidths at Ka-band.

Summing up all the loss contributions, the study finds an overall efficiency of 62.4% in the best-case scenario with a corresponding loss value of 2.05 dB. The worst-case scenario shows an efficiency of 41.9% and a loss value of 3.77 dB. The 1.7-dB additional loss in the worst-case scenario is attributed to three factors: 0.5 dB due to a poorer panel set, 0.9 dB due to offset pointing, and 0.3 dB due to imperfect gravity compensation.

It should be stressed that all the computed values are likely the best case and actual, real-world implementations will incur additional loss. This is discussed further in the next section.

Table 3. Summary of Best- and Worst-Case Losses, 32.3 GHz.

RMS Contributor	Best Efficiency	Best Loss (dB)	Worst Efficiency	Worst Loss (dB)	Fixed Quantity
Physical Optics	0.9200	0.3621	0.9200	0.3621	Fixed Quantity
Quadri pod Blockage	0.9200	0.3621	0.9200	0.3621	Fixed Quantity
Mirror Ruze Loss	0.8266	0.8270	0.8266	0.8270	Best: 0.25 mm Worst 0.35 mm
Primary Panel Set	0.8918	0.4976	0.7989	0.9752	Best: 45° Worst: 17.3°
Gravity Compensation	1.0000	0.0000	0.9230	0.3480	Best: OnPoint Worst: 2FWHM
Pointing	1.0000	0.0000	0.8128	0.9002	Fixed Quantity
Total	0.6239	2.0489	0.4193	3.7747	

XII. Conclusion

Based on the simulations described in the report, the gravity losses and pointing issues involved with operating the DSN 70-m antennas at Ka-band are likely manageable, but additional work is required to move forward. The program office would ideally provide a strawman set of requirements that are consistent with the assumptions made in the futures study.[1] The requirements should include details on what bands need to be operating simultaneously with Ka-band. It is likely that an entire cone would need to be dedicated to

Ka-band equipment, requiring some existing capabilities to be eliminated. An alternative would be complete redesign of the tri-cone area to create more usable volume. This decision will involve a complicated trade-off between cost and future capability.

The next step would be the development of a detailed mechanical layout of the Ka-band optics. Assuming the flat DM option is selected, a detailed mechanical design of the flat DM and new gravity compensation calculations, which include its limitations, need to be completed. Improvement of the current panel set on the 70 m is a very important topic. Holography and setting capable of producing a 0.25-mm surface must be pursued. Ideally, a panel setting of this quality would be demonstrated on one of the 70-m antennas and checked periodically for stability. The pointing studies reported here show that vernier pointing can be accomplished with a flat mirror. If this method is used to accomplish differential pointing of the Ka-band transmit and receive beams, it is important to have a requirement on the differential pointing angles that need to be accommodated so that worst-case transmit gain losses can be computed. This requirement will depend on future missions and the associated spacecraft trajectories.

Acknowledgments

The author acknowledges the support of Steve Lichten from the DSN program office for providing the system-level motivation leading to this study. The holography data that was used in this modeling effort was provided by Alberto Torre and Manuel Vázquez of the Madrid Deep Space Communications Complex and is greatly appreciated. Eric Gama provided valuable help on the mechanical details of the 70-m surfaces and dimensions, and finally Behrouz Khayatian provided excellent technical feedback on the content of this report.

References

[1] P. D. Potter, "64-Meter Antenna Operation at KA-Band," Telecommunications and Data Acquisition Progress Report: Volume 42-57, Jet Propulsion Laboratory, Pasadena, California, pp. 65-70, June 15, 1980. http://ipnpr.jpl.nasa.gov/progress_report/42-57/57K.PDF

[2] TICRA GRASP Software, https://www.ticra.com/software/grasp/, accessed September 11, 2025.

[3] Alberto Torre and Manuel Vazquez, “Connected-Element Interferometer Holography via Correlation of Signals from the Common Platform,” *Interplanetary Network Progress Report: Volume 42-241*, Jet Propulsion Laboratory, Pasadena, California, pp. 1-19, May 15, 2025. https://ipnpr.jpl.nasa.gov/progress_report/42-241/42-241D.pdf

[4] J. Antebi, M. S. Zarghamee, F. W. Kan, H. Hartwell, J. E. Salah and S. M. Milner, “A deformable sub-reflector for the Haystack radio telescope,” *IEEE Antennas and Propagation Magazine*, vol. 36, no. 3, pp. 19-28, June 1994.

[5] D. J. Hoppe, “A Study of Deformable-Mirror Performance Versus Actuator Distribution Using an Influence-Function Model,” *Interplanetary Network Progress Report: Volume 42-147*, Jet Propulsion Laboratory, Pasadena, California, pp. 1-14, November 15, 2001. https://ipnpr.jpl.nasa.gov/progress_report/42-147/147E.pdf

[6] D. J. Hoppe, "The Sensitivity of Main-Reflector-Distortion Compensation to Deformable-Mirror Position," Telecommunications and Mission Operations Progress Report: Volume 42-145, Jet Propulsion Laboratory, Pasadena, California, pp. 1-13, May 15, 2001. https://ipnpr.jpl.nasa.gov/progress_report/42-145/145I.pdf

[7] “Antenna Positioning,” DSN Document 810-005, 302, Rev. E , July 1, 2024. https://deepspace.jpl.nasa.gov/dsndocs/810-005/302/302E.pdf